Observation of Room-Temperature Magnetoresistance in Monolayer MoS_2 by Ferromagnetic Gating

Wenjing Jie,[1,2] Zhibin Yang,[1] Fan Zhang,[1] Gongxun Bai,[1] Chi Wah Leung,[1] and Jianhua Hao[1*]

[1]Department of Applied Physics, The Hong Kong Polytechnic University, Hung Hom, Kowloon, Hong Kong, China

[2]College of Chemistry and Materials Science, Sichuan Normal University, Chengdu, 610068, China

***Corresponding author: jh.hao@polyu.edu.hk**

ABSTRACT

Room-temperature magnetoresistance (MR) effect is observed in wafer-scale MoS_2 layers coupled with ferromagnetic dielectric $CoFe_2O_4$ (CFO). Through the ferromagnetic gating, MR ratio of -12.7% can be experimentally achieved in monolayer MoS_2 under 90 kOe at room temperature. Such observed MR effect is attributed to the spin accumulation and injection from the MoS_2/CFO interface into the MoS_2 layer by spin coupling effect. The injected spin may contribute to the spin current induced by the spin Hall effect and eventually change the resistance of MoS_2 itself because of inverse spin Hall effect. The observed MR ratio is much higher than that in previously reported nonmagnetic metal coupled with magnetic insulator which generally exhibited MR ratio of less than 1%. The anisotropic MR effect enhances dramatically as the thickness of MoS_2 decreasing down to monolayer, while the MR ratio becomes negligible in MoS_2 with more than 10 layers. Our research provides an insight into exploring room-temperature MR in monolayer materials, which should be helpful for developing a new generation of ultra-thin magnetic storage devices in the atomically-thin limit.

KEYWORDS: wafer –scale; monolayer MoS_2; $CoFe_2O_4$; heterostructures; magnetoresistance

INTRODUCTION

Magnetoresistance (MR) is the change in electrical resistance of materials induced by the external magnetic field, i.e., the response of electrical resistance to a magnetic field. Large MR, for example, giant MR (GMR) was discovered in multilayers of alternating ferromagnetic and nonmagnetic metalic thin films,[1,2]while colossal MR (CMR) generally occurs in manganese-based perovskite oxides.[3,4] Besides, extremely large MR was reported in several semimetals, such as Dirac semimetal of Cd_3As_2 with linear band crossing at the Fermi level, resonant compensated semimetal of WTe_2 with perfect electron–hole symmetry and Weyl semimetal of LaSb due to the breaking of time reversal symmetry.[5–7] Among them, WTe_2, a layered transition metal dichalcogenide (TMD), shows large non-saturating MR and shares the record of highest MR ratio with LaSb and NbP.[8,9] The first-principles calculations suggested that the extraordinary MR effect could be maintained in its two-dimensional (2D) form.[10] Very recently, the magnetic transport and spin-orbit coupling have been studied in atomically thin WTe_2 layers.[11–14] However, the MR measurements were generally performed at extremely low temperature, and the metal-insulator transition limited the feasibility of measuring MR in ultra-thin WTe_2 layers. Nevertheless, these earlier investigations have already brought MR phenomenon to the 2D layered form. Unfortunately, most studies on 2D materials remain constrained to studying electronic, photonic and optoelectronic properties,[15–17] while much less experimental work has been reported on spintronics as well as MR behaviors.

It is noticeable that MoS_2, as a prototypical TMD material, was reported to exhibit a gate-induced superconducting state in monolayer form at a critical temperature of 2 K.[18] Previous studies also show that MoS_2 possess strong spin-orbit coupling and potential large spin-orbit torques when coupling with magnetic alloy/metal.[19–21] However, the magnetic conductors could

cause short circuit in the adjacent MoS_2 layers and subsequently restrict the electrical measurements of the MoS_2 layers. Thus, combing 2D materials with ferromagnetic dielectrics is highly desirable. In this work, wafer-scale monolayer (1L) and multilayer (ML) MoS_2 samples were integrated with ferromagnetic $CoFe_2O_4$ (CFO) to explore the spin coupling effects. The electrical resistance of the prepared MoS_2 sample is found to be tuned by the magnetization existed in the adjacent CFO thin film at room temperature (RT). The results provide one opportunity to investigate the spin generation and modulation in monolayer sample by ferromagnetic gating.

RESULTS AND DISCUSSION

To fabricate the wafer-scale MoS_2/CFO heterostructures, pulse laser deposition (PLD) method was employed to grow 1L and ML MoS_2 samples as well as the CFO thin films. In our previous works, both epitaxial CFO thin films and 2D layered materials can be well deposited by PLD method. [22–24] High-quality CFO thin films were well deposited on single-crystal MgO substrates (see Supporting Information, Figure S1). Subsequently, MoS_2 layers were deposited on CFO/MgO simply by rotating targets from CFO to MoS_2 without breaking vacuum. It was reported that wafer-scale 2D MoS_2 samples could be deposited on various substrates through the Van der Waals epitaxy by PLD technique.[25,26] In this work, the prepared samples are analyzed by x-ray diffraction (XRD) technique, as shown in Figure 1a. (002) diffraction peak indicates the formation of *c*-axis oriented MoS_2 layers. Furthermore, the fabricated MoS_2 samples were etched off and transferred onto a copper gird for characterizations of transmission electron microscope (TEM). The selected area electron diffraction (SAED) pattern with incident zone axis ⟨001⟩ of the MoS_2 is shown in the inset of Figure 1a. The diffraction pattern clearly shows two circles with lattice spaces of 0.27 nm and 0.16 nm, corresponding the (100) and (110) planes of the

MoS_2 in the circle patterns, respectively. The polycrystalline behaviors of the prepared MoS_2 samples are evident by the circle patterns for both planes. The layer number of the fabricated MoS_2 samples can be precisely determined by the cross-sectional high-resolution TEM (HR-TEM) image. Accordingly, the deposition rate of PLD-grown MoS_2 is calculated to be about 55 laser pulses per layer. Figure 1b shows the cross-sectional view of 3-layer (3L), 2-layer (2L) and 1L MoS_2 samples grown on CFO/MgO. A layered structure of the prepared MoS_2 samples and the distinct interface between the PLD-grown CFO and MoS_2 samples can be clearly seen from the HR-TEM cross-sectional images. Therefore, 2D layered MoS_2 samples are *c*-axis oriented with random in-plane orientation.

Moreover, micro-Raman is a powerful method to characterize 2D materials. It is well known that the positions of E_{2g} and A_{1g} peaks as well as the distance between them can be used as criteria of determining the layer number of the MoS_2 layers.[27] As shown in Figure 1c, the frequency of E_{2g} peak decreases while the A_{1g} increases as increasing layer number, i.e., the two peaks shift close to each other from the distance of about 25 cm^{-1} for 5-layer (5L) MoS_2 to 18 cm^{-1} when the thickness decreasing to monolayer. Next, as shown in Figure 1d, three-dimensional Raman mapping image of 1L MoS_2 sample demonstrates feature peaks of E_{2g} and A_{1g} over an area of 10 μm × 10 μm. Both feature peaks appear in the overall image with a nearly uniform intensity and distance between them of about 18 cm^{-1}, implying that a continuous monolayer MoS_2 has been deposited on the CFO thin film. Furthermore, x-ray photoelectron spectroscopy (XPS) was used to investigate the chemical states of Mo and S in monolayer samples, as shown in Figure 1e and f. The binding energies located at 161.7 and 162.8 eV are of S $2p_{3/2}$ and S $2p_{1/2}$, for S^{2-} in MoS_2, respectively. The binding energies of Mo $3d_{3/2}$ and Mo $3d_{5/2}$ locate at 232.0 and 228.8 eV, respectively, corresponding to Mo^{4+} in MoS_2. The absence of the

peak at around 235.6 eV for $3d_{5/2}$ suggests no Mo^{6+} resulted from MoO_3,[28,29] ruling out the possible oxidation of the fabricated MoS_2 layers in air and/or chemical reaction with the underling CFO thin film. Based on all aforementioned characterizations, we can conclude that the continuous, uniform 1L and ML MoS_2 layers can be well deposited on the CFO thin films. The detailed information of fabrication and characterizations is shown in the experimental section.

In the MR measurements, the van der Pauw geometry is fabricated, which is generally used for the MR characterizations of 2D materials.[30] As schematically shown in Figure 2a, the longitudinal resistance of 1L MoS_2, named R_{xx} ($R_{xx} = V_{xx}/I_{xx}$.), is recorded by measuring the longitudinal voltage ($V_{xx} = V_{out} - V_{in}$) when the current ($I_{xx}$) flows along the longitudinal direction with or without the external magnetic field (H). The MR ratio (MR_{xx}) is defined as the change of longitudinal resistance divided by resistance under 0 kOe, that is $\Delta R_{xx}/R_{xx}(H = 0)$, where $\Delta R_{xx} = R_{xx}(H) - R_{xx}(H = 0)$. $H_{//}$ and H_T stand for H is applied in the MoS_2 plane, parallel and perpendicular to I_{xx}, respectively, while $H_\perp$ means the H is normal to the MoS_2 plane. Considering the MoS_2 layer possesses relatively good conductivity as well as the underlying CFO thin films are dielectric materials with high permittivity, the CFO thin films should not divert electric current away from MoS_2 layer (see Supporting Information, Figure S2). Herein, the changes of resistance originate from the response to H of MoS_2 samples. As an example for illustrating MR effect, R_{xx} of one 1L MoS_2 sample was measured by the physical property measurement system (PPMS) under an external H. Figure 2b shows the temperature-dependent R_{xx} of one 1L MoS_2 sample with and without H. As temperature decreasing, the resistance increases dramatically, suggesting the semiconducting behavior for PLD-grown 1L MoS_2. The resistance becomes too large to be measurable by the PPMS when the temperature is below

about 20 K. A slight decrease of resistance can be observed when H is applied. To be more specific, as shown in Figure 2c and d, 1L MoS_2 shows an obvious resistance change under H at the temperature from 300 down to 100 K. R_{xx} decreases when increasing H in both positive and negative directions. Therefore, negative MR_{xx} is achieved, about -9.17% for H_T (top panel in Figure 2c) under 40 kOe at 300 K. Furthermore, a butterfly-shape hysteresis loop with the MR_{xx} of -7.57% is observed in the curve for $H_\perp$ (top panel in Figure 2d). As temperature decreasing from 300 to 100 K, the MR gradually drops to -5.19% for H_T and -2.99% for $H_\perp$.

To further understand the physical mechanism, the magnetic properties of the CFO thin films as well as MoS_2/CFO heterostructures were studied by the vibrating sample magnetometer (VSM) measurement system on the PPMS. Figure 3a shows the H dependence of the in-plane and out-of-plane magnetization (M) in CFO recorded at RT. It should be noted that no additional magnetization signals were detected in MoS_2/CFO heterostructure compared to CFO thin film according to VSM results. The out-of-plane loop indicates a typical ferromagnetic behavior with a coercive field of about 2.3 kOe and a saturation field of about 12 kOe, while the in-plane magnetic measurement shows a very slim hysteresis loop with a small coercive field near to zero, suggesting the perpendicular anisotropy in the PLD-deposited CFO thin films. It is interesting to find the field range in which resistance shows butterfly-shape curve for 1L MoS_2 coincides with the saturated magnetization field of CFO thin film. Especially, when magnetic field is applied perpendicular to the MoS_2 plane, the more visible butterfly-shape curve of MoS_2 corresponds to the enhanced magnetization in CFO thin film. As the temperature decreasing, the butterfly-shape area is enlarged, which is consistent to the enhanced magnetization in the underlying CFO when the measured temperature decreases from 300 to 100 K (see Supporting Information Figure S3). The observation indicates the MR effects in MoS_2 layers may generate from the coupling effect

with the underlying magnetic CFO. For comparison, the resistance changes of 1L MoS_2 samples directly grown on nonmagnetic SiO_2/Si or MgO substrates without CFO thin films between MoS_2 samples and the substrates are measured, respectively. In fact, no MR behaviors can be observed in both cases at RT, as shown in Figure 3b. Thus, the MR effect observed in MoS_2/CFO heterostructure is expected to be attributed to the coupling effect deriving from the underling ferromagnetic CFO thin film, which is consistent with earlier studies about nonmagnetic metal integrated with ferromagnetic insulaor.[31]

There are two possible physical mechanisms to address the observed MR behaviors in the heterostructure. The first one is proposed that the MR effect is likely to originate from proximity-induced or/and the vacancy-induced magnetism in the MoS_2 layer. It was reported that local spin generation and modulation in graphene might be controlled by a nearby magnetic insulator of EuS.[32] And the ferromagnetism was theoretically and experimentally reported in graphene coupled with a magnetic insulator, for example, yttrium iron garnet (YIG) thin film, via magnetic proximity effect (MPE). [33,34] The MPE relies on the generated magnetic moments across the interface into the nonmagnetic materials (metals and graphene).[33,35] In the aforementioned VSM data, no additional magnetization signals is detected in MoS_2/CFO heterostructure compared to CFO thin film, suggesting the fabricated MoS_2 layers cannot provide additional magnetic moments. Besides, it was reported that S vacancies could induce the transforming from semiconducting (2H) MoS_2 to semimetal (1T) MoS_2 with ferromagnetic properies.[36] Indeed, PLD-grown MoS_2 layers are semiconducting, even when *H* is applied, according to the behaviors in temperature-dependent resistance. This measurement can rule out the possibility of phase transition from 2H to 1T. Thus, on the other hand, the MR behaviors detected in 1L MoS_2 samples may result from the spin Hall magnetoresistance (SMR). The ferromagnetic CFO is

likely to generate spin accumulated at the interface of MoS_2/CFO, which could give contribution to the spin current in the 2D layer. The SMR is the resistance changes depending on H generated from the spin Hall effect and inverse spin Hall effect (SHE and ISHE).[37] The SHE refers to the generation of a pure spin current (J_s) transverse to the electron current (J_e) occurs in paramagnetic systems in the absence of H due to the spin-orbit interaction.[38,39] Then, the spin accumulation at the transverse two sides gives rise to the spin current in the opposite transversal direction, i.e. the ISHE. The inverse spin current gives contribution to the J_e along the longitudinal direction. As schematically shown in Figure 4a, when an electron current J_e is applied in the longitudinal direction (x), J_s can be generated in the transverse direction (y) in the 1L MoS_2 sample. The J_s is considered as a distribution of a current with spin-up electrons in one direction and a current with spin-down electrons in the opposite direction. On the contrary, the spin in the two opposite directions can combine to form J_{sback} with the opposite direction to the J_s, and consequently induce the electron current J_{se} with the same direction to the applied J_e. The induced J_{se} can inevitably contribute to the conductivity of the MoS_2 layer. However, the value of J_{se} is generally too small to be detected in experiments. When the MoS_2 layer is adjacent to the ferromagnetic CFO thin film and the external filed is applied, spin generation and accumulation can be formed at the interface. And the accumulated spin will be injected from the interface into the MoS_2 layer via the spin coupling and contribute to J_s as well as J_{se}, which eventually induces the MR effect in MoS_2 layer.

Furthermore, the R_{xx} as a function of the sweeping angle (θ) was measured when H is swept from $H_\perp$ to H_T or from $H_\perp$ to $H_{//}$ in the range of 0 to 360 °, as exhibited in Figure 4b top and bottom panel, respectively. A nearly periodic change is exhibited with H from $H_\perp$ to H_T, while the change becomes negligible when H is swept from $H_\perp$ to $H_{//}$. Herein, the behaviors of H

intensity- and direction-dependent resistance are evident for 1L MoS_2 sample combined with CFO thin film. For the direction sweeping, H is much larger than the magnetization saturation field. This means the magnetization is aligned with H over the whole sweeping period. When H is swept from $H_\perp$ to H_T, the relationship between R_{xx} and θ can be fitted to the following equation:

$$R_{xx} = R_{xxT} + \frac{1}{2}(R_{xx\perp} - R_{xxT})\sin[\frac{\pi(\theta+45)}{90}] \quad (1)$$

i.e., $$\Delta R_{xx} = (R_{xx\perp} - R_{xxT})\cos^2(\omega) \quad (2)$$

Hence, ΔR_{xx} displays $\cos^2(\omega)$ (where ω is equal to $2\pi\theta$ /360) dependence which is expected for SMR, as shown by the red curve. This dependence is consistent with the previous reports on nonmagnetic metal by ferromagnetic insulating gating.[40] However, the SMR exhibits no directional dependence when H is swept from $H_\perp$ to $H_{//}$, as shown in the bottom panel of Figure 4b. The SMR is tuned by the angle of the spin accumulation to H. Hence, when the H is swept from $H_\perp$ to $H_{//}$, the resistance will remain unchanged. Therefore, the observed MR behaviors in 1L MoS_2 samples can be attributed to the coupling effects with the underlying CFO.

By considering the MR effect in MoS_2 is caused by spin contribution in the vicinity of the CFO thin film, MR should saturate along with the saturated magnetization of CFO. However, it should be noted that the MR of 1L MoS_2 shows no signature of saturation at RT under 40 kOe where CFO already saturates. Even when H_T reaches up to the maximum of 90 kOe, the 1L MoS_2 sample demonstrates no saturation behaviors with a MR value of -12.7%, as shown in top panel of Figure 4c. Besides, the relationship between R_{xx} and the sweeping angle of H when it is fixed at 90 kOe is shown in the bottom panel of Figure 4c. Similar to the aforementioned sweeping H of 40 kOe, R_{xx} exhibits $\cos^2(\omega)$ relationship with sweeping angle, as shown by the

fitted red curve. Actually, the magnetization of the measuring configuration (CFO/MgO) exhibits a nearly linear curve under high field when taking large diamagnetic contribution from the underlying substrate into consideration (see Supporting Information Figure S4). The large diamagnetic response generally should be removed by subtracting the linear part under high magnetic field to obtain the magnetization data of CFO thin film. This process unavoidably eliminates the linear contribution from the CFO thin film under high field. Therefore, the presence of non-saturated behaviors of the SMR in 1L MoS_2 should be attributed to non-saturated magnetization in the CFO thin film under high magnetic field. Such non-saturated MR combined with saturated magnetization was also reported in Pt/CFO heterostructure.[37] Importantly, this is a very high value particularly measured at RT, compared to the previously reported nonmagnetic metal thin films whose spin generated MR effect is very weak, generally the ratio is less than 1%.[31,41,42] Such an intense RT MR effect might be related to the unique 2D layered structure whose surface without dangling bonds or trap states.[43]

To further confirm the point, the transverse resistance (R_{xy}, the measured voltage, V_{xy}, is perpendicular to the I_{xx}) is recorded in the monolayer MoS_2 sample. When H is applied perpendicular to the sample plane, a hysteresis loop is demonstrated in the H-dependent R_{xy} curves, as shown in Figure 4d. This is due to the hysteresis magnetization of the underlying CFO, as shown in Figure 3a. The magnetic moments in CFO are arranged along the direction of H and keep almost constant when H is in excess of the coercive field of the CFO. As a consequence, R_{xy} keeps almost constant at this stage. Then, the dramatic change of magnetization in CFO can induce the resistance change in MoS_2 layer when the direction of H changes. In terms of the case for H sweeping from positive to negative, a sharp transition can be formed around H = 0 kOe and vice vista. The transition in R_{xy} corresponds to the magnetization switch in the CFO. Therefore,

the H-dependent R_{xy} shows a hysteresis loop which is consistent to the H-dependent magnetization of CFO. This also can prove MR behaviors in MoS_2 layers are mainly generated from the coupling to the underlying CFO thin films.

Moreover, multilayer MoS_2 samples were prepared on CFO to form the heterostructures for investigation of the coupling effects between MoS_2 and CFO. As an example for illustrating MR effect in multilayer samples, MR behaviors of one 3L MoS_2 sample at RT under H_T and $H_\perp$ are demonstrated in Figure 5. 3L MoS_2 shows an obvious resistance change, although the resistance shows relative weak dependence on H. Analogous to the behaviors in 1L samples, R_{xx} decreases under H. Herein, negative MR_{xx} is achieved for the 3L sample, about -0.5% for H_T (top panel in Figure 5) at RT under 40 kOe. Similarly, a butterfly-shape hysteresis loop is observed in the curve for $H_\perp$ (bottom panel in Figure 5). In this work, there is no observable MR effect in thick (more than 10L) MoS_2 layers deposited on the CFO thin films. Therefore, it can be proposed that the anisotropic MR effect enhances dramatically as the thickness of MoS_2 decreasing down to 1L, while the MR ratio becomes negligible in MoS_2 with more than 10 layers. The absence of MR effect in thick MoS_2 layers also can rule out the possibilities of either electromagnetic artifacts, or the magnetized MoS_2 layer responsible for the observed MR behaviors.

CONCLUSIONS

In summary, MR effect is experimentally observed in 2D MoS_2 ultra-thin layers coupled with ferromagnetic CFO thin films at RT. MR effect is negligible when the thickness beyond 10 layers for MoS_2, while enhanced dramatically as thickness decreasing to monolayer, where the MR ratio can reach up to the value of -12.7%. The MR ratio is much higher than that in previously reported nonmagnetic metal coupled with magnetic insulator which generally

exhibited MR ratio of less than 1%. The observed MR effect is attributed to the spin accumulation and injection from the MoS_2/CFO interface into the MoS_2 layers by the spin coupling. The injected spin can contribute to the spin current and eventually change the resistance of MoS_2 layers. The absence of MR in MoS2 prepared on SiO_2/Si and MgO substrates, and the angle-independent R_{xx} with H sweeping from $H_{\perp}$ to $H_{//}$ as well as the hysteresis loop in R_{xy} can further support that the observed MR is generated from the coupling effects with the underlying CFO. Our results based on wafer-scale MoS_2/CFO heterostructures pave the way for developing ultra-thin data storage devices in the 2D limit at RT.

METHODS

Fabrication of MoS_2/CFO heterostructures: Both CFO and MoS_2 thin films were prepared by PLD method with an operation pulse laser of KrF (λ=248 nm). The PLD method used here for making the heterostructure provides two main advantages for the heterostructure. Firstly, this method offers good contact between MoS_2 and CFO, which is better than conventional transferring method and subsequently beneficial to creating spin coupling. Secondly, MoS_2 samples can be *in-situ* grown on CFO thin films in vacuum without the exposure of CFO to air avoiding potential contaminations. In our experiments, high-quality CFO thin films were well deposited on single-crystal MgO substrates by PLD method by considering the very small lattice mismatch between them (see Supporting Information, Figure S1). The CFO thin films were deposited with a substrate temperature of 650 ºC and a deposition vacuum of 5×10^{-5} Pa. During the deposition, laser energy was controlled to be 250 mJ and the pulse frequency of 1 Hz. Then, the subsequent *in situ* annealing was performed in an oxygen atmosphere at 500 ºC for 30 min to minimize potential oxygen vacancies during the deposition process. Then the film was cooled

down to RT and kept in vacuum up to 1×10^{-5} Pa for the subsequent MoS_2 ultra-thin layer deposition. MoS_2 layers were deposited on CFO/MgO simply by rotating targets from CFO to MoS_2 without breaking vacuum. For MoS_2 growth, the substrate was heated to 600 ºC in a base vacuum of 1×10^{-5} Pa. Then MoS_2 thin film was deposited at a deposition vacuum of about 3×10^{-5} Pa and a growth temperature of 600 °C. The laser energy was controlled to be 100 mJ and the pulse frequency of 5 Hz.

Characterizations: High resolution x-ray diffractometer (XRD, Rigaku, SmartLab, 9 kW) and atomic force microscope (AFM, DI Nanocope 8) were employed to characterize the orientation and the surface morphology of both the CFO thin films and MoS_2 layers, respectively. The interface characterizations of CFO/MgO as well as CFO/MoS_2 were performed by high resolution transmission electron microscope (TEM, Bruker Nano). Besides, the prepared MoS_2 layers were characterized using Raman spectroscopy (HORIBA JOBIN YVON, HR800) with the excitation wavelength of 488 nm. The prepared samples were also detected by XPS measurements equipped with a Twin anode (Al/Mg) X-ray sources. And the measurements were performed by a SKL-12 spectrometer modified with VG CLAM 4 multichannel hemispherical analyzer. All binding energies were calibrated with the C 1s peak located at 284.8 eV in this work. In a physical property measurement system (PPMS, Model 6000 by Quantum Design), the resistance signals were achieved by recording the measured voltage divided by the applied current when an in-plane or out-of-plane magnetic field up to 90 kOe was applied to the heterostructure. Besides, the magnetic properties of the CFO thin films were studied by the vibrating sample magnetometer (VSM) measurement system in the PPMS.

ASSOCIATED CONTENT

XRD, AFM, and TEM images of the CFO thin films; The current-voltage curves of the MoS_2; Magnetic hysteresis loops of CFO thin film at 300, 150, and 100 K; Magnetic hysteresis loops of the CFO thin film by considering the contribution from substrate of MgO. This material is available free of charge via the Internet at http://pubs.acs.org.

AUTHOR INFORMATION

Corresponding Author

*E-mail: jh.hao@polyu.edu.hk.

ORCID

Jianhua Hao: 0000-0002-6186-5169

ACKNOWLEDGEMENT

This work was supported by the grants from Research Grants Council of Hong Kong (GRF No. PolyU 153031/15P), Collaborative Research Fund (CRF No. HKU9/CRF/13G, PolyU Grant No. E-RD5), PolyU Internal Grant (1-ZE14), and National Natural Science Foundation of China (No. 61604100).

REFERENCES

(1) Baibich, M. N.; Broto, J. M.; Fert, A.; Van Dau, F. N.; Petroff, F.; Eitenne, P.; Creuzet, G.; Friederich, A.; Chazelas, J. Giant Magnetoresistance of (001)Fe/(001)Cr Magnetic Superlattices. *Phys. Rev. Lett.* **1988**, *61*, 2472–2475.

(2) Felser, C.; Fecher, G. H.; Balke, B. Spintronics: A Challenge for Materials Science and Solid-State Chemistry. *Angew. Chem. Int. ed.* **2007**, *46*, 668–699.

(3) Helmolt, R. von; Wecker, J.; Holzapfel, B.; Schultz, L.; Samwer, K. Giant Negative Magnetoresistance in Perovskitelike La2/3Ba1/3MnOx Ferromagnetic Films. *Phys. Rev. Lett.* **1993**, *71*, 2331–2333.

(4) Jin, S.; Tiefel, T. H.; McCormack, M.; Fastnacht, R. a; Ramesh, R.; Chen, L. H. Thousandfold Change in Resistivity in Magnetoresistive La-ca-Mn-O Films. *Science* **1994**, *264*, 413–415.

(5) Tafti, F. F.; Gibson, Q. D.; Kushwaha, S. K.; Haldolaarachchige, N.; Cava, R. J. Resistivity Plateau and Extreme Magnetoresistance in LaSb. *Nat. Phys.* **2015**, *12*, 272–277.

(6) Ali, M. N.; Xiong, J.; Flynn, S.; Tao, J.; Gibson, Q. D.; Schoop, L. M.; Liang, T.; Haldolaarachchige, N.; Hirschberger, M.; Ong, N. P.; *et al.* Large, Non-Saturating Magnetoresistance in WTe2. *Nature* **2014**, *514*, 205–208.

(7) Liang, T.; Gibson, Q.; Ali, M. N.; Liu, M.; Cava, R. J.; Ong, N. P. Ultrahigh Mobility and Giant Magnetoresistance in the Dirac Semimetal Cd3As2. *Nat. Mater.* **2014**, *14*, 280–284.

(8) Jiang, J.; Tang, F.; Pan, X. C.; Liu, H. M.; Niu, X. H.; Wang, Y. X.; Xu, D. F.; Yang, H. F.; Xie, B. P.; Song, F. Q.; *et al.* Signature of Strong Spin-Orbital Coupling in the Large Nonsaturating Magnetoresistance Material WTe2. *Phys. Rev. Lett.* **2015**, *115*, 166601.

(9) Rhodes, D.; Das, S.; Zhang, Q. R.; Zeng, B.; Pradhan, N. R.; Kikugawa, N.; Manousakis, E.; Balicas, L. Role of Spin-Orbit Coupling and Evolution of the Electronic Structure of WTe 2 under an External Magnetic Field. *Phys. Rev. B* **2015**, *92*, 125152.

(10) Lv, H.; Lu, W.; Shao, D.; Liu, Y. Perfect Charge Compensation in WTe2 for the Extraordinary Magnetoresistance: From Bulk to Monolayer. *Eur. Lett.* **2014**, *110*, 37004.

(11) Wang, L.; Gutiérrez-Lezama, I.; Barreteau, C.; Ubrig, N.; Giannini, E.; Morpurgo, A. F. Tuning Magnetotransport in a Compensated Semimetal at the Atomic Scale. *Nat.*

Commun. **2015**, *6*, 8892.

(12) MacNeill, D.; Stiehl, G. M.; Guimaraes, M. H. D.; Buhrman, R. A.; Park, J.; Ralph, D. C. Control of Spin-Orbit Torques through Crystal Symmetry in WTe2/ferromagnet Bilayers. *Nat. Phys.* **2016**, DOI: 10.1038/NPHYS3933.

(13) Wang, Y.; Liu, E.; Liu, H.; Pan, Y.; Zhang, L.; Zeng, J.; Fu, Y.; Wang, M.; Xu, K.; Huang, Z.; *et al.* Gate-Tunable Negative Longitudinal Magnetoresistance in the Predicted Type-II Weyl Semimetal WTe2. *Nat. Commun.* **2016**, *7*, 13142.

(14) Zhang, E.; Chen, R.; Huang, C.; Yu, J.; Zhang, K.; Wang, W.; Liu, S.; Ling, J.; Wan, X.; Lu, H.-Z.; *et al.* Tunable Positive to Negative Magnetoresistance in Atomically Thin WTe2. *Nano Lett.* **2016**, DOI: 10.1021/acs.nanolett.6b04194.

(15) Novoselov, K. S.; Geim, A. K.; Morozov, S. V.; Jiang, D.; Zhang, Y.; Dubonos, S. V.; Grigorieva, I. V.; Firsov, A. A. Electric Field Effect in Atomically Thin Carbon Films. *Science* **2004**, *306*, 666–669.

(16) Jie, W.; Chen, X.; Li, D.; Xie, L.; Hui, Y. Y.; Lau, S. P.; Cui, X.; Hao, J. Layer-Dependent Nonlinear Optical Properties and Stability of Non-Centrosymmetric Modification in Few-Layer GaSe Sheets. *Angew. Chem. Int. ed.* **2015**, *54*, 1185–1189.

(17) Samad, L.; Bladow, S. M.; Ding, Q.; Zhuo, J.; Jacobberger, R. M.; Arnold, M. S.; Jin, S. Layer-Controlled Chemical Vapor Deposition Growth of MoS2 Vertical Heterostructures via van Der Waals Epitaxy. *ACS Nano* **2016**, *10*, 7039–7046.

(18) Costanzo, D.; Jo, S.; Berger, H.; Morpurgo, A. F. Gate-Induced Superconductivity in Atomically Thin MoS2 Crystals. *Nat. Nanotechnol.* **2015**, *11*, 339–344.

(19) Xiao, D.; Liu, G. Bin; Feng, W.; Xu, X.; Yao, W. Coupled Spin and Valley Physics in Monolayers of MoS 2 and Other Group-VI Dichalcogenides. *Phys. Rev. Lett.* **2012**, *108*,

196802.

(20) Zhang, W.; Sklenar, J.; Hsu, B.; Jiang, W.; Jungfleisch, M. B.; Xiao, J.; Fradin, F. Y.; Liu, Y.; Pearson, J. E.; Ketterson, J. B.; *et al.* Research Update: Spin Transfer Torques in Permalloy on Monolayer MoS2. *APL Mater.* **2016**, *4*, 32302.

(21) Shao, Q.; Yu, G.; Lan, Y.-W.; Shi, Y.; Li, M.-Y.; Zheng, C.; Zhu, X.; Li, L.-J.; Amiri, P. K.; Wang, K. L. Strong Rashba-Edelstein Effect-Induced Spin–Orbit Torques in Monolayer Transition Metal Dichalcogenide/Ferromagnet Bilayers. *Nano Lett.* **2016**, *16*, 7514−7520.

(22) Huang, W.; Zhu, J.; Zeng, H. Z.; Wei, X. H.; Zhang, Y.; Li, Y. R.; Hao, J. H. Effect of Strain on the Ferroelectric Properties in Epitaxial Perovskite Titanate Thin Films Grown on Ferromagnetic CoFe2O4 Layers. *Scr. Mater.* **2008**, *58*, 1118–1120.

(23) Yang, Z.; Hao, J.; Yuan, S.; Lin, S.; Yau, H. M.; Dai, J.; Lau, S. P. Field-Effect Transistors Based on Amorphous Black Phosphorus Ultrathin Films by Pulsed Laser Deposition. *Adv. Mater.* **2015**, *27*, 3748–3754.

(24) Yang, Z.; Jie, W.; Mak, C.-H.; Lin, S.; Lin, H.; Yang, X.; Yan, F.; Lau, S. P.; Hao, J. Wafer-Scale Synthesis of High-Quality Semiconducting Two-Dimensional Layered InSe with Broadband Photoresponse. *ACS Nano* **2017**, DOI: 10.1021/acsnano.7b01168.

(25) Wang, S.; Yu, H.; Zhang, H.; Wang, A.; Zhao, M.; Chen, Y.; Mei, L.; Wang, J. Broadband Few-Layer MoS2 Saturable Absorbers. *Adv. Mater.* **2014**, *26*, 3538–3544.

(26) Serna, M. I.; Yoo, S. H.; Moreno, S.; Xi, Y.; Oviedo, J. P.; Choi, H.; Alshareef, H. N.; Kim, M. J.; Minary-Jolandan, M.; Quevedo-Lopez, M. A. Large-Area Deposition of MoS2 by Pulsed Laser Deposition with in Situ Thickness Control. *ACS Nano* **2016**, *10*, 6054–6061.

(27) Li, H.; Zhang, Q.; Yap, C. C. R.; Tay, B. K.; Edwin, T. H. T.; Olivier, A.; Baillargeat, D. From Bulk to Monolayer MoS 2: Evolution of Raman Scattering. *Adv. Funct. Mater.* **2012**, *22*, 1385–1390.

(28) Lin, Y.; Chen, R.; Chou, T.; Lee, Y.; Chen, Y.; Chen, K.; Chen, L. Thickness-Dependent Binding Energy Shift in Few- Layer MoS 2 Grown by Chemical Vapor Deposition. *ACS Appl. Mater. Interfaces* **2016**, *8*, 22637–22646.

(29) Ho, Y. T.; Ma, C. H.; Luong, T. T.; Wei, L. L.; Yen, T. C.; Hsu, W. T.; Chang, W. H.; Chu, Y. C.; Tu, Y. Y.; Pande, K. P.; *et al.* Layered MoS2 Grown on c -Sapphire by Pulsed Laser Deposition. *Phys. Status Solidi - Rapid Res. Lett.* **2015**, *9*, 187–191.

(30) Lu, J.; Zhang, H.; Shi, W.; Wang, Z.; Zheng, Y.; Zhang, T.; Wang, N.; Tang, Z.; Sheng, P. Graphene Magnetoresistance Device in van Der Pauw Geometry. *Nano Lett.* **2011**, *11*, 2973–2977.

(31) Nakayama, H.; Althammer, M.; Chen, Y. T.; Uchida, K.; Kajiwara, Y.; Kikuchi, D.; Ohtani, T.; Geprägs, S.; Opel, M.; Takahashi, S.; *et al.* Spin Hall Magnetoresistance Induced by a Nonequilibrium Proximity Effect. *Phys. Rev. Lett.* **2013**, *110*, 206601.

(32) Wei, P.; Lee, S.; Lemaitre, F.; Pinel, L.; Cutaia, D.; Cha, W.; Katmis, F.; Zhu, Y.; Heiman, D.; Hone, J.; *et al.* Strong Interfacial Exchange Field in the graphene/EuS Heterostructure. *Nat. Mater.* **2016**, *15*, 711.

(33) Yang, H. X.; Hallal, A.; Terrade, D.; Waintal, X.; Roche, S.; Chshiev, M. Proximity Effects Induced in Graphene by Magnetic Insulators: First-Principles Calculations on Spin Filtering and Exchange-Splitting Gaps. *Phys. Rev. Lett.* **2013**, *110*, 46603.

(34) Wang, Z.; Tang, C.; Sachs, R.; Barlas, Y.; Shi, J. Proximity-Induced Ferromagnetism in Graphene Revealed by the Anomalous Hall Effect. *Phys. Rev. Lett.* **2015**, *114*, 16603.

(35) Huang, S. Y.; Fan, X.; Qu, D.; Chen, Y. P.; Wang, W. G.; Wu, J.; Chen, T. Y.; Xiao, J. Q.; Chien, C. L. Transport Magnetic Proximity Effects in Platinum. *Phys. Rev. Lett.* **2012**, *109*, 107204.

(36) Cai, L.; He, J.; Liu, Q.; Yao, T.; Chen, L.; Yan, W.; Hu, F.; Jiang, Y.; Zhao, Y.; Hu, T.; *et al.* Vacancy-Induced Ferromagnetism of MoS_2 Nanosheets. *J. Am. Chem. Soc.* **2015**, *137*, 2622–2627.

(37) Valvidares, M.; Dix, N.; Isasa, M.; Ollefs, K.; Wilhelm, F.; Rogalev, A.; Sánchez, F.; Pellegrin, E.; Bedoya-Pinto, A.; Gargiani, P.; *et al.* Absence of Magnetic Proximity Effects in Magnetoresistive Pt/CoFe2O4 Hybrid Interfaces. *Phys. Rev. B* **2016**, *93*, 214415.

(38) Valenzuela, S. O.; Tinkham, M. Direct Electronic Measurement of the Spin Hall Effect. *Nature* **2006**, *442*, 176–179.

(39) Kato, Y. K.; Myers, R. C.; Gossard, A. C.; Awschalom, D. D. Observation of the Spin Hall. *Science* **2004**, *306*, 1910–1913.

(40) Grigoryan, V. L.; Guo, W.; Bauer, G. E. W.; Xiao, J. Intrinsic Magnetoresistance in Metal Films on Ferromagnetic Insulators. *Phys. Rev. B* **2014**, *90*, 161412(R).

(41) Kim, J.; Sheng, P.; Takahashi, S.; Mitani, S.; Hayashi, M. Spin Hall Magnetoresistance in Metallic Bilayers. *Phys. Rev. Lett.* **2016**, *116*, 97201.

(42) Isasa, M.; Bedoya-Pinto, A.; Vélez, S.; Golmar, F.; Sánchez, F.; Hueso, L. E.; Fontcuberta, J.; Casanova, F. Spin Hall Magnetoresistance at Pt/CoFe2O4 Interfaces and Texture Effects. *Appl. Phys. Lett.* **2014**, *105*.

(43) Liu, Y.; Weiss, N. O.; Duan, X.; Cheng, H.-C.; Huang, Y.; Duan, X. Van Der Waals Heterostructures and Devices. *Nat. Rev. Mater.* **2016**, *490*, 16042.

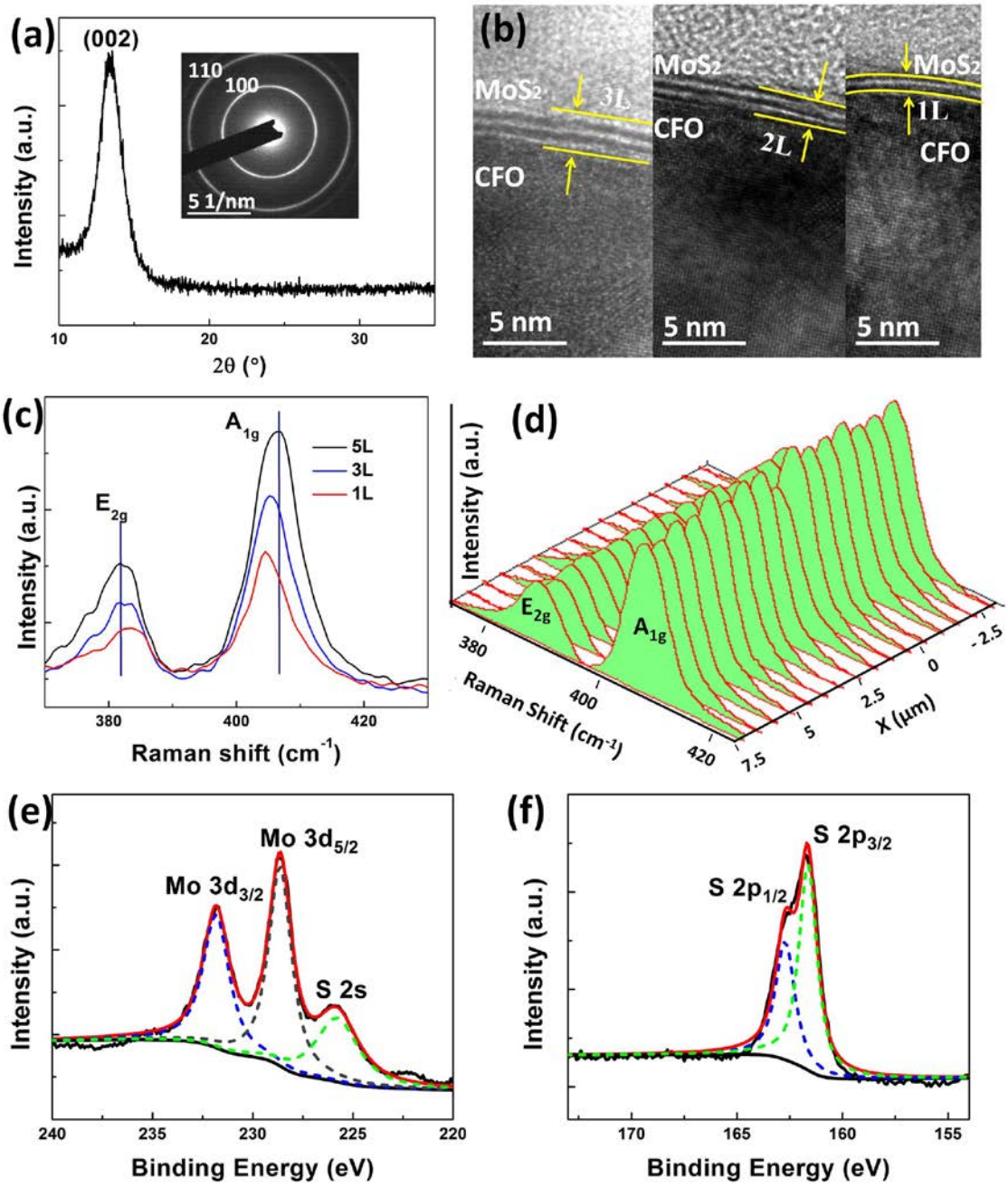

Figure 1. Characterizations of PLD-grown MoS_2 samples. (a) XRD 2θ scanning pattern of MoS_2 sample. The inset shows the SAED pattern of the MoS_2 sample. (b) Cross-sectional TEM images of MoS_2/CFO heterostructures with MoS_2 samples of 3L, 2L and 1L. (c) Layer-dependent Raman spectra of layered MoS_2 thin films with layer number of 1, 3, and 5. (d) Three-dimensional Raman mapping image of monolayer PLD-grown MoS_2 onto CFO over an area of

10 μm × 10 μm. XPS spectra of Mo 3d and S 2s (e) as well as S 2p (f) for monolayer MoS_2 layer onto CFO/MgO.

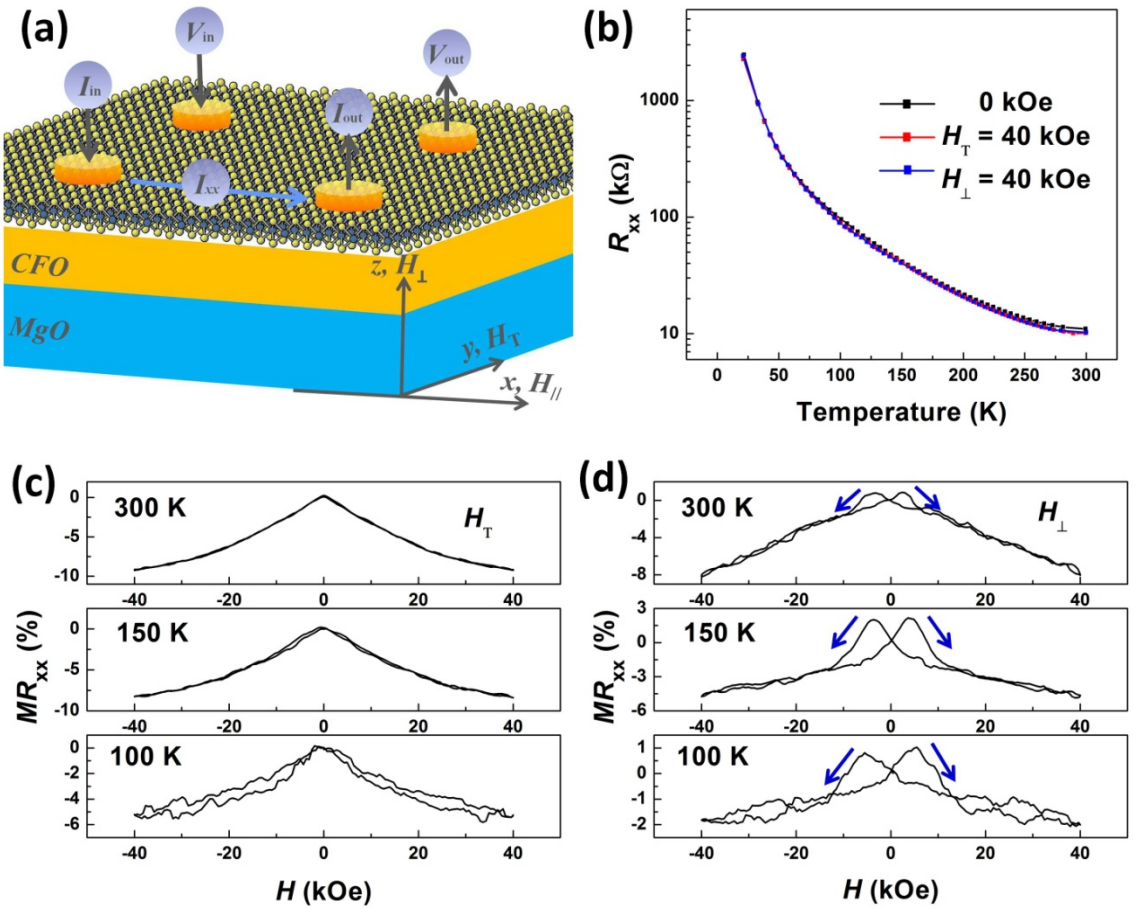

Figure 2. MR measurements of monolayer MoS_2. (a) Schematics of the the MoS_2/CFO heterostructure and the van der Pauw geometry. (b) Temperature-dependent resistance without *H* as well as the *H* is applied transverse to the electron current in the MoS_2 plane and perpendicular to the MoS_2 plane both with the value of 40 kOe. (c) The MR behaviors of 1L MoS_2 sample when the *H* is applied in the direction of transverse to the electric current in the MoS_2 plane at 300, 150 and 100 K, respectively. (d) The MR behaviors of 1L MoS_2 when the *H* is applied perpendicular to the MoS_2 plane at 300, 150 and 100 K, respectively.

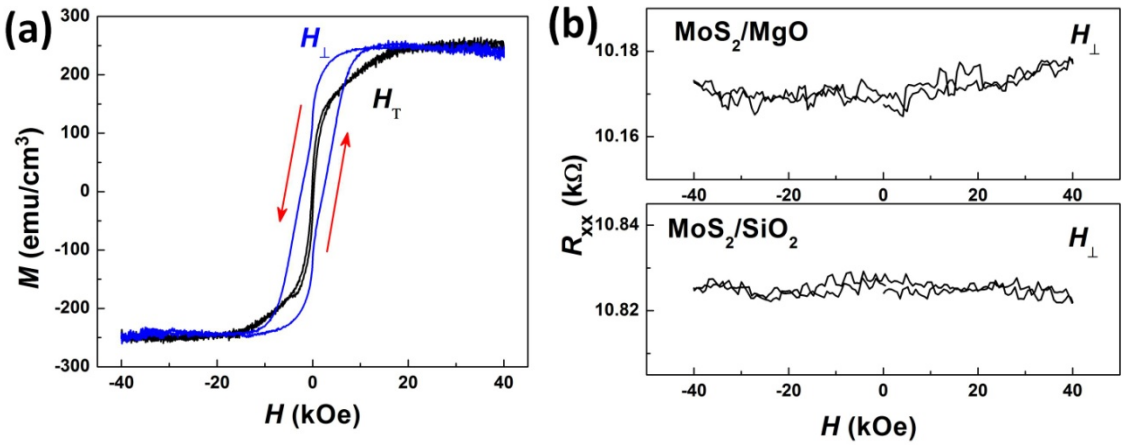

Figure 3. (a) Magnetic hysteresis loops of the CFO sample grown on single-crystal MgO substrate when the magnetic field is applied in the CFO plane transverse to the electric current (black loop) or perpendicular to the CFO plane (blue loop). (b) The resistance of monolayer MoS_2 directly grown on MgO and SiO_2/Si substrates as a function of *H* when it is applied perpendicular to the MoS_2 plane.

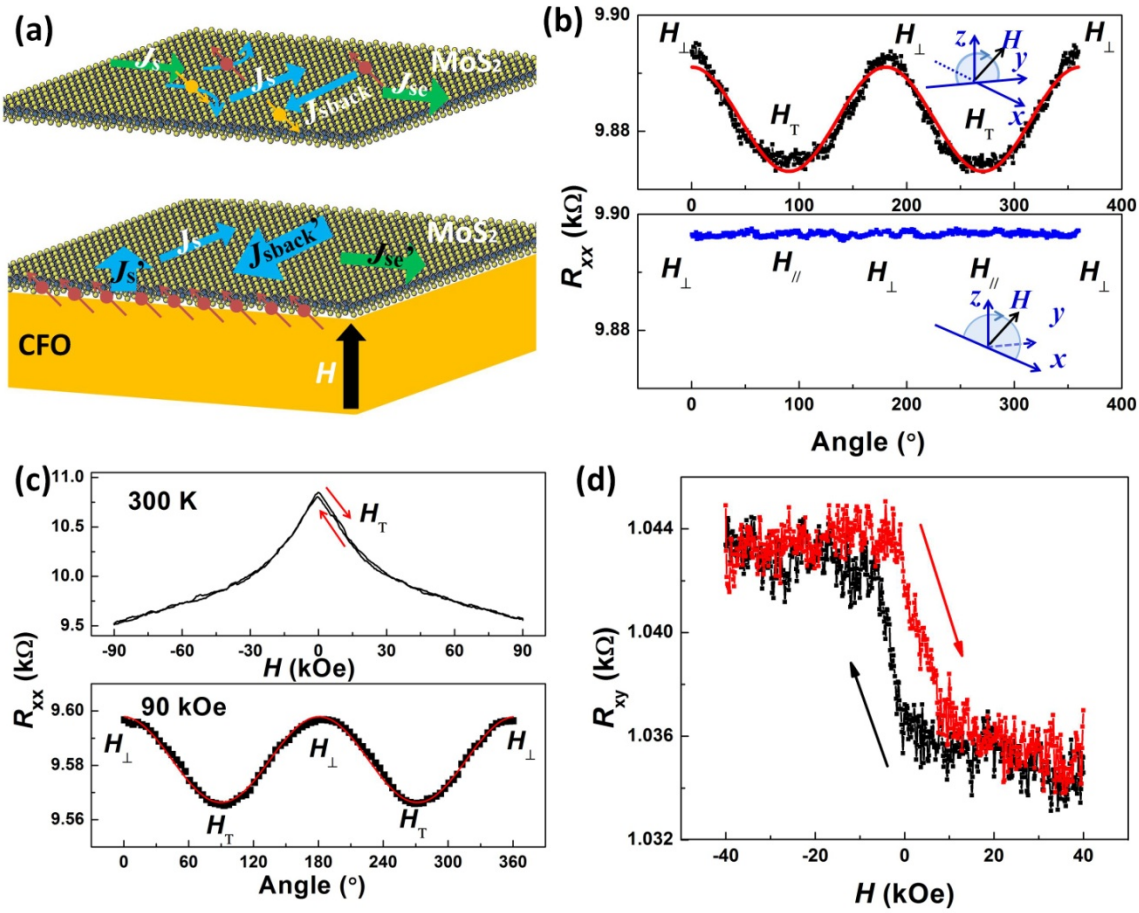

Figure 4. (a) Schematics of the mechanism of SMR in the MoS_2/CFO heterostructure. (b) The *H*-direction-dependent resistance of 1L MoS_2 when *H* is fixed at 40 kOe. Top: the *H* is swept from *z*-direction (that is the normal to the MoS_2 plane) to *y*-direction (i.e., transverse to the current direction). Bottom: the *H* is swept from the *z*-direction to the *x*-direction (i.e., the current direction). (c) Top: The *H*-dependent resistance of monolayer MoS_2 when *H* is applied transverse to the electron current direction. Bottom: the angle-dependent resistance when *H* is fixed at 90 kOe and swept from *z*- to *y*-direction. (d) The transverse resistance of 1L MoS_2 as a function of *H* when it is applied perpendicular to the sample plane.

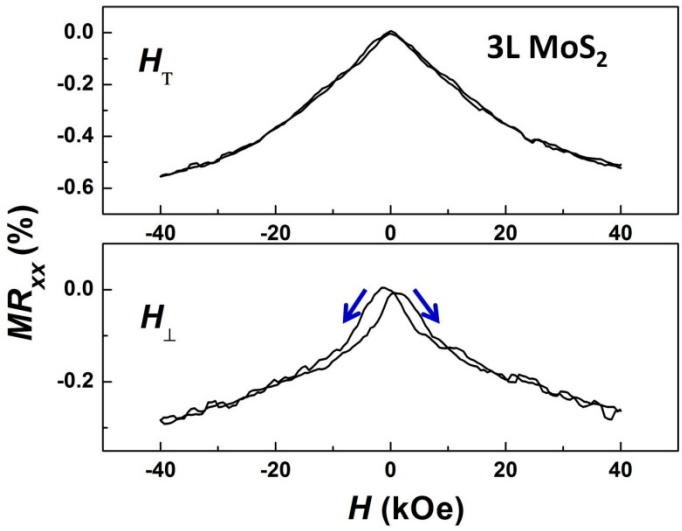

Figure 5. MR measurements for 3L MoS_2. The *H*-dependent MR ratio of 3L MoS_2 when the *H* is applied transverse to the electric current in the MoS_2 plane or perpendicular to the MoS_2 plane.

TABLE OF CONTENT (TOC) GRAPHICS: